Escola de Primavera de Transição e Turbulência
Blumenau 2022

ABCM
13th Spring School on Transition and Turbulence
September 19th-23rd, 2022, Blumenau, SC, Brazil

EPTT-2022-0005

TIDAL TURBINE PERFORMANCE PREDICTION ACCOUNTING FOR TRANSITION

Luís Henrique da Silva Ignacio
School of Mechanical Engineering, Federal University of Uberlândia, Av. João Naves de Ávila, 2121 Bloco 5P, Uberlândia, Minas Gerais, Brazil
luis.henrique@ifgoiano.edu.br

Carlos Antonio Ribeiro Duarte
Federal University of Catalão, Faculty of Engineering, Av. Dr. Lamartine Pinto de Avelar, 1120, Catalão, Goiás, Brazil.
carlosduarte@ufcat.edu.br

Francisco José de Souza
School of Mechanical Engineering, Federal University of Uberlândia, Av. João Naves de Ávila, 2121 Bloco 5P, Uberlândia, Minas Gerais, Brazil
francisco.souza@ufu.br

Abstract. *In this work, the analysis of the power coefficient of a SeaGen turbine in 1:25 scale was performed. This procedure is fundamental in the turbine development and/or improvement process and is largely performed through the Blade Element Momentum (BEM) methodology, which is applied in QBlade software and its starting point are the curves of drag and lift coefficients as a function of the angle of attack. The Reynolds number to obtain such curves was defined as that occurs in the cross section located at a position equal to 70% of the blade span. In addition, for the NACA 63-618 aerodynamic profile, which is applied along the entire blade span of SeaGen turbine, the Langtry-Menter Shear Stress Transport (LM-SST) transitional turbulence model was applied and showed a good agreement with experimental results. Before assessing the turbine power curve, the lift and drag curves were treated with AERODAS model, which estimates the pre-stall and post-stall lift and drag values. The power curve obtained presented a good approximation with the experimental. Therefore, all the necessary steps for a relatively simple and low cost turbine energy evaluation are detailed.*

Keywords: *NACA 63-618, LM-SST, AERODAS, turbine power curve, transitional turbulence model.*

1. INTRODUCTION

The development of a wind or current turbine project, from its first model to its production, is marked by some analysis stages, such as: aerodynamic, structural and cost. A project like this is characterized by the equilibrium of several quantities, such as efficiency, resistance, vibration and cost (Song and Lubitz, 2013; Barnes *et al.*, 2015; Liu *et al.*, 2017; Fingersh *et al.*, 2006). Obviously, the aim of the project is for the most efficient and resistant, and that presents the lowest vibration and cost, respecting the design conditions.

When mentioning the cost of a turbine, it is important to emphasize that the project development phase also generates expenses, and one of the main is linked to time. For example, the people involved are remunerated, that is, every fraction of their work time has a cost. Thus, if less time is spent on the project, the total cost of the turbine is reduced. This facilitates the dissemination of this technology, as it allows a greater number of people to access it.

One of the stages of the turbine design is the aerodynamic analysis. Basically, at this stage the main focus is the definition of the blade geometry (rotor radius, aerodynamic profile, chord, pitch and twist angles) to capture as much energy as possible, respecting the design conditions. In this phase, the forces acting on the turbine are also calculated, which will be the basis for the structural analysis. To simulate the aerodynamic characteristics of the turbine, two methods can be highlighted: Computational Fluid Dynamics (CFD) and Blade Element Momentum (BEM).

Computational Fluid Dynamics (CFD) is an important tool that enables the simulation of fluid-structure interaction, through the solution of the Navier-Stokes partial differential equations (Bai and Wang, 2016). The solution of such equations allows analyzing the aerodynamic behavior of the structure by obtaining the fields of pressure and flow velocity. Despite being a methodology whose physical basis is quite robust, its application for turbine simulation presents high computational times, because it is necessary to use very refined three-dimensional meshes and, even so, the simulation of boundary layer separation is a challenge (Lanzafame *et al.*, 2013).

Sezer-Uzol and Long (2006) applied CFD to simulate a complete revolution of the National Renewable Energy Laboratory (NREL) Phase VI turbine. They used multiple clusters and varied the number of processors. The lowest times obtained were with the National Center Computer Applications (NCSA) cluster at the University of Illinois, which spent 10 days to complete the simulation with 16 processors and 1.7 days with 128 processors.

The Blade Element Momentum (BEM) is based on the combination of momentum and blade element theories (Bran-

lard, 2017). In practice, this methodology divides the turbine blade into "N" parts and calculates for each of them the relative velocity (V_{rel}) of the fluid and the respective angle of attack (Cao, 2011). Thus, as the drag and lift curves as a function of the angle of attack (α) for the applied airfoil are provided, the drag (C_D) and lift (C_L) coefficients are obtained and the forces acting on the section are calculated. Numerical integration along the blades span allows calculating the performance of the turbine (Ingram, 2005). BEM stands out for enabling, in a quick and practical way, the alteration of the turbine geometry and the evaluation of its performance for a wide range of fluid velocities (Lanzafame and Messina, 2007). All this, with simulation times ranging from a few seconds to minutes (Bai and Wang, 2016). Therefore, are evident the reasons that make BEM the methodology most applied by industries (Song and Lubitz, 2013; Carcangiu, 2008; Lanzafame and Messina, 2007).

As mentioned, it is necessary to provide the curves of the drag and lift coefficients as a function of the angle of attack, which can be obtained by experiment or CFD two-dimensional simulation (Bai and Wang, 2016). As simulation is generally the cheapest option, choose the appropriate turbulence model is essential to reproduce what happens in practice and, consequently, has a direct influence on the quality of turbine power estimation. In addition, some corrections must be applied to the $C_D \times \alpha$ and $C_L \times \alpha$ curves, as three-dimensional effects that occur during turbine operation are not considered due to the curves being obtained by two-dimensional models (Carcangiu, 2008; Lanzafame and Messina, 2007).

In this study, all the necessary steps for the turbine energy evaluation will be detailed: from the simulation of $C_D \times \alpha$ and $C_L \times \alpha$ curves, until obtaining the power curve in the QBlade software (Marten *et al.*, 2013).

2. METHODOLOGY

This section will introduce some fundamental concepts for the evaluation of the power coefficient (C_P). Therefore, first of all, it is necessary to understand the concept of this dimensionless coefficient. Its calculation is carried out by the ratio between the power extracted by the turbine and that available in the fluid that flows around the blade, as shown in Eq. (1).

$$C_P = \frac{P_{extracted}}{0.5\,\rho\,A\,U_\infty^3} \tag{1}$$

where $P_{extracted}$ is the power converted by the rotor, ρ is the specific mass of the fluid considered, A is the area swept by the rotor and U_∞ is the free stream velocity.

The calculation of the extracted power will be carried out through the BEM in the QBlade software. Briefly and chronologically, for the application of BEM, the curves of drag and lift coefficients as a function of the angle of attack must be provided. Such curves will be obtained by simulations performed in the UNSCYFL3D software. Before inserting such curves in QBlade, they will be treated with the AERODAS model, which estimates the pre and post-stall C_D and C_L. Finally, after these steps, the turbine power coefficient curve is obtained in QBlade sofgtware, which is generally presented as a function of the tip speed ratio (TSR), which is calculated by:

$$TSR = \frac{\omega\,R}{U_\infty} \tag{2}$$

where ω is the angular velocity and R is the rotor radius.

2.1 Blade Element Momentum - BEM

BEM is obtained from the combination of two theories: momentum and blade element theory. The first uses an annular control volume to apply conservation of linear and angular momentum and thus equate thrust and torque, which are, respectively, presented by Eqs. (3) and (4) (Manwell *et al.*, 2002).

$$dT_{MT} = F4\pi r\rho U_\infty^2 a(1-a)dr\ cos^2(\delta) \tag{3}$$

$$dQ_{MT} = F4\pi r^3\rho U_\infty^2(1-a)a'\,\omega\,dr\ cos^4(\delta) \tag{4}$$

where F is the total loss factor, r is the radius at any blade element, a is the axial induction factor, a' is the tangential induction factor, and δ is the cone angle.

On the other hand, the blade element theory considers the blade geometry to analyze its aerodynamic forces to also equate thrust and torque, as shown in Eqs. (5) and (6) (Pratumnopharat and Leung, 2011)

$$dT_{BET} = \frac{1}{2}\rho BcV_{rel}^2(C_L cos(\phi) + C_D sin(\phi))dr\ cos(\delta) \tag{5}$$

$$dQ_{BET} = \frac{1}{2}\rho B c V_{rel}^2 (C_L sin(\phi) - C_D cos(\phi)) r\, cos(\delta)\; dr \tag{6}$$

where B is the number of blades, c is the chord length, V_{rel} is the relative flow velocity, a is the axial induction factor, a' is the tangential induction factor, and ϕ is the inflow angle (see Fig. 1-(b)).

Equating the expressions obtained for thrust and torque by each theory, expressions to calculate the axial induction factors (a), which represents how much the fluid velocity is reduced by the presence of the rotor, and tangential (a') are obtained (Puraca, 2019). Such equations are presented in Eqs. (7) and (8).

$$a = \frac{1}{\frac{4Fsin^2(\phi)}{\sigma cos^2(\delta)(C_L cos(\phi) + C_D sin(\phi))} + 1} \tag{7}$$

$$a' = \frac{1}{\frac{4Fsin(\phi)cos(\phi)}{\sigma(C_L sin(\phi) - C_D cos(\phi))} - 1} \tag{8}$$

where $\sigma = \frac{Bc}{2\pi r cos(\delta)}$ is a solidity ratio.

The methodology application is carried out by an iterative process, in which the blade is divided into several sections, as shown in Fig. 1-(a). Starting from an initial guess for a and a', the normal and tangential velocities and, consequently, the relative velocity are calculated. Subsequently, the inflow angle (ϕ) is calculated, and as the pitch and torsion angles are already known, the angle of attack (α) is calculated using the expression: $\alpha = \phi - (twist + pitch)$, as shown in Fig. 1-(b). With the value of α and using the provided curves of $C_D \times \alpha$ and $C_L \times \alpha$, C_D and C_L are obtained. Using Eqs. (7) and (8) recalculates a and a'. The process then restarts from the calculation of normal, tangential and relative velocities and is interrupted when the value of α converges. Such procedure must be performed for each of the "N" sections that the blade has been split. Finally, a numerical integration of the forces acting on the blade, calculated using the C_D and C_L of each section, is performed, and the power extracted by the blade is obtained (Branlard, 2017).

It is also important to highlight the need to insert corrections to the method for greater precision in power estimates, such as tip and hub losses (Branlard, 2017; Carcangiu, 2008; Lanzafame and Messina, 2007).

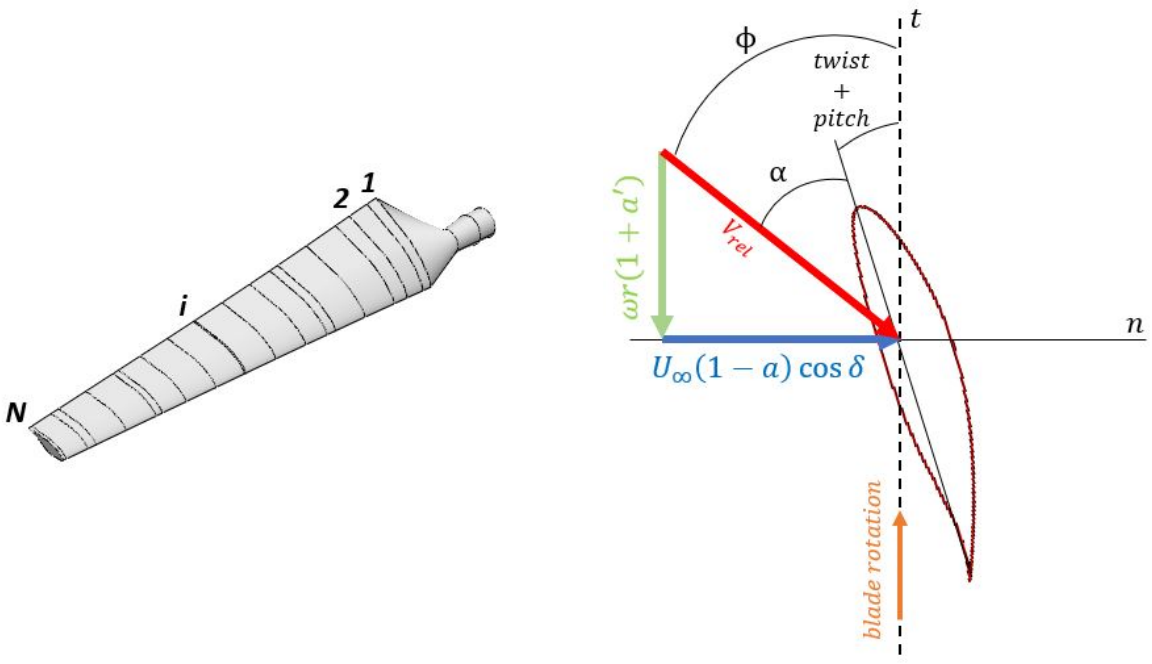

(a) Blade divided into "N" sections.

(b) Angles and velocities for the application of the iterative process.

Figure 1. BEM relevant parameters.

2.2 Drag and Lift Coefficients

NACA 63-618 is the aerodynamic profile applied by Walker *et al.* (2014) in the 1:25 scale construction of SeaGen turbine. These authors performed two-dimensional experiments to obtain the curves of drag and lift coefficients as a function of the angle of attack for Reynolds numbers equal to 4.2×10^5, 5.3×10^5, and 1.0×10^6, calculated with Eq. (9). Such equation is based on the chord length (c), which in this study is equal to $0.23\ m$, and on the relative velocity (V_{rel}).

$$Re_c = \frac{\rho\, V_{rel}\, c}{\mu} \tag{9}$$

where μ is the dynamic viscosity.

The present work carried out simulations for $Re_{c,70\%.s} = 4.0 \times 10^5$, because according to Walker *et al.* (2014) this is the Reynolds that occur in 70% of the blade span (s). As turbulence model, the Langtry-Menter Shear Stress Transport (LM-SST) was applied, because Ignacio *et al.* (2020) showed that this model presented the results of C_D and C_L closer to the experimental for NACA 63-618. All simulations were performed in UNSCYFL3D software.

The two-dimensional meshes were generated in ICEM CFD 16.0©, which all dimensions are based on the chord length (c), as shown in Fig. 2-(a). Based on aerofoil coordinates obtained from AirfoilTools (2022), more points were generated for the leading and trailing edge regions, as shown in Fig. 2-(b). As these regions has more complex geometry, it can affect the mesh design and consequently the simulation results. It is worth noting that only the vertical line downstream of the airfoil was defined as outlet (pressure outlet), and all others defined as inlet (velocity inlet).

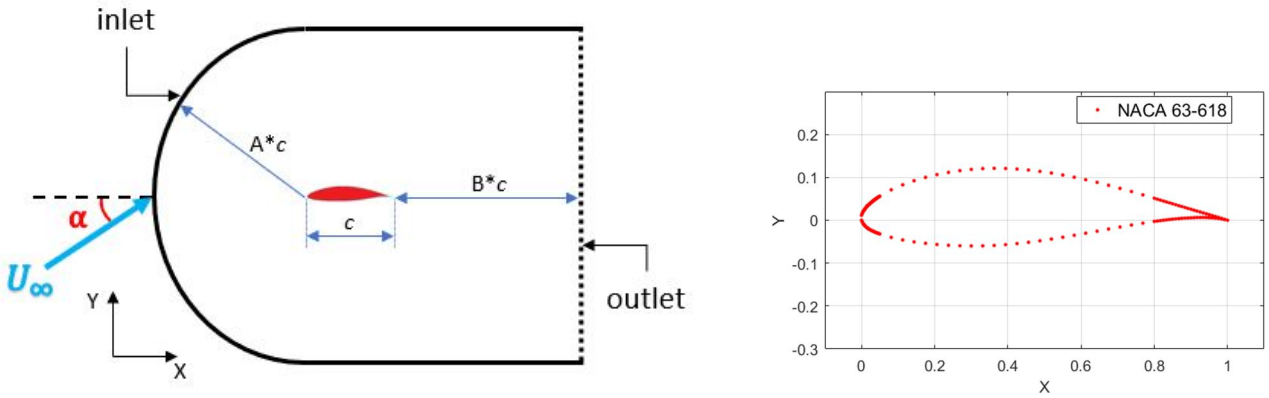

(a) Schematic representation. (b) Airfoil region.

Figure 2. Details to generate the mesh.

Four meshes were generated, whose configuration is shown in Tab. 1. For each mesh the distance from the airfoil to the far-field boundaries (A and B values - see Fig. 2-a), the height of the first mesh cell (Δy) or the type (number of points) were varied. It is important to note that some definitions were based on the study of Coder (2018), as highlighted in Tab. 1. This author defines $\Delta y = 6.5 \times 10^{-6} * c$ and the leading and trailing edge spacing equal to $10^{-3} * c$ and $5 \times 10^{-4} * c$, respectively.

Table 1. Important values for mesh design.

Mesh	A	B	Δy [m]	y^+	Type$^{(1)}$
1	20	25	$1.27 \times 10^{-}5$	1	-
2	1000$^{(1)}$	1000$^{(1)}$	$1.49 \times 10^{-}6^{(1)}$	0.1176	Medium$^{(1)}$
3	20	25	$1.49 \times 10^{-}6^{(1)}$	0.1176	Medium$^{(1)}$
4	20	25	$1.49 \times 10^{-}6^{(1)}$	0.1176	Extra-Fine$^{(1)}$

$^{(1)}$ Coder (2018)

2.3 Aerodas

Developed by Spera (2008), Aerodas is a mathematical model that allows to calculate the drag and lift coefficients of an aerodynamic profile for pre-stall and post-stall regimes, as the blades can operate in both aerodynamic regimes. Thus, it is possible to obtain the complete curves of $C_D \times \alpha$ and $C_L \times \alpha$, necessary to apply the BEM.

The starting point of such methodology are the C_D and C_L pre-stall values, as they are easily obtained in the literature or by simulation. Unlike other extrapolation methodologies, such as Viterna (Viterna and Janetzke, 1982) and Montgomerie (Montgomerie, 2004), which consider that the airfoil behaves like a flat plate in the post-stall, the Aerodas equations for the post-stall were obtained empirically, based on data available for some airfoils.

Therefore, it is important to know how to identify the stall phenomenon in the $C_L \times \alpha$ curve. When the angle of attack is increased, the tendency is that the same happens with the coefficient C_L. However, from a certain angle (α_{stall}), this trend is not maintained and there is a drop in lift and a abrupt increase in drag (White, 2011).

As mentioned before, the starting point for the application of Aerodas are the curves of drag and lift coefficients in pre-stall regime. The imput parameters are extracted from them, as shown in Fig. 3. The definition of each one of them is presented in Tab. 2. It is important to note that all values related to the pre-stall have the number 1 in their acronym, while for the post-stall the number 2 is used.

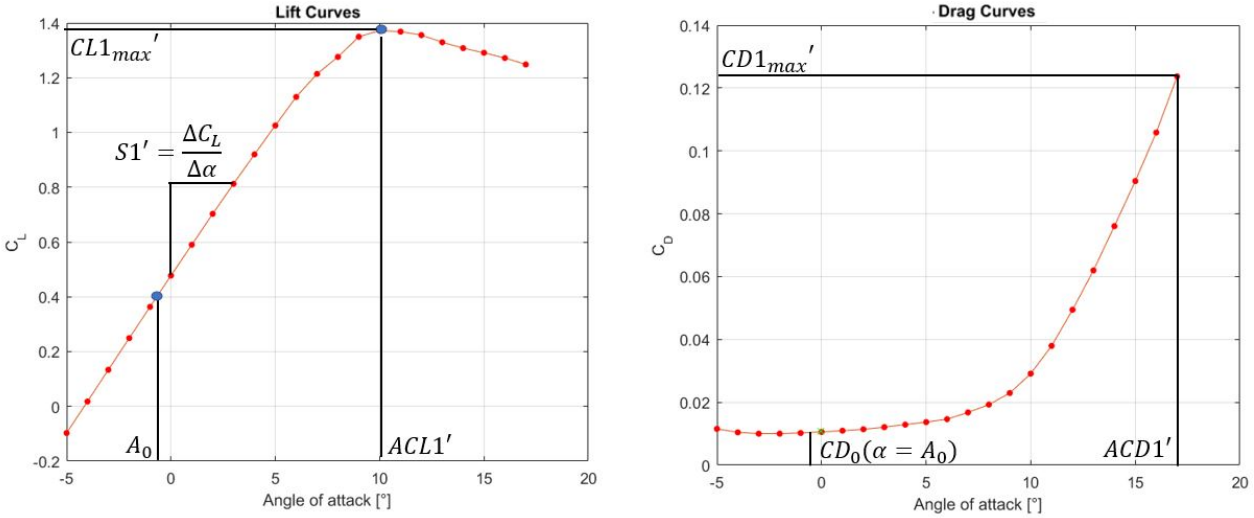

Figure 3. Aerodas important pre-stall values.

Table 2. Definition of Aerodas input parameters.

Parameter	Definition
A0	α for $C_L = 0$ [deg]
$CL1_{max}{}'$	maximum C_L
ACL1$'$	α for $C_{L1_{max}}{}'$ [deg]
CD0	C_D for α =A0
$CD1_{max}{}'$	maximum C_D
ACD1$'$	α for $C_{D1_{max}}{}'$ [deg]
$S1'$	slope of linear segment of lift curve [1/deg]

As the data obtained for the airfoils are obtained by two-dimensional simulations or experiments, that is, they consider an infinite length, they must be corrected to take into account a finite length of the blade. Such correction is performed using the aspect ratio (AR), calculated applying Eqs. (10) and (11).

$$R_m = \sqrt{\frac{R_{tip}^2 + R_{inner}^2}{2}} \tag{10}$$

where R_{tip} is the tip radius and R_{inner} is the radius of inner end of active airfoil.

$$AR = \frac{2(R_{tip} - R_{inner})}{c_m} \tag{11}$$

where c_m is the chord length at R_m.

Corrections are carried out with Eqs. (12) - (16).

$$ACL1 = ACL1^{'} + 18.2 \cdot CL1_{max}{}^{'} \cdot AR^{-0.9} \tag{12}$$

$$CL1_{max} = CL1_{max}{}^{'} (0.67 + 0.33 \cdot e^{-(4/AR)^2}) \tag{13}$$

$$ACD1 = ACD1^{'} + 18.2 \cdot CL1_{max}{}^{'} \cdot AR^{-0.9} \tag{14}$$

$$CD1_{max} = CD1_{max}{}^{'} + 0.280 \cdot (CL1_{max}{}^{'})^2 \cdot AR^{-0.9} \tag{15}$$

$$S1 = \frac{S1^{'}}{1 + 18.2 \cdot S1' \cdot AR^{-0.9}} \tag{16}$$

Equations (17) - (19) are applied for lift and drag pre-stall coefficients.

$$CL1 = S1 \cdot (\alpha - A0) - RCL1 \cdot \left(\frac{\alpha - A0}{ACL1 - A0} \right)^{N_1}, \quad \textbf{if } \alpha \geq A0 \tag{17}$$

$$CL1 = S1 \cdot (\alpha - A0) - RCL1 \cdot \left(\frac{A0 - \alpha}{A0 - ACL1} \right)^{N_1}, \quad \textbf{if } \alpha < A0 \tag{18}$$

where $RCL1 = S1 \cdot (ACL1 - A0) - CL1_{max}$ and $N_1 = 1 + \frac{CL1_{max}}{RCL1}$.

$$CD1 = CD0 + (CD1_{max} - CD0) \cdot \left(\frac{\alpha - A0}{ACD1 - A0} \right)^{M}, \quad \textbf{if } (2A0 - ACD1) \leq \alpha \leq ACD1 \tag{19}$$

where M must be determined by fitting Eq. (19) to the graph $\frac{C_L}{C_D} \times \alpha$.

For the post-stall regime, the lift and drag coefficients are calculated by Eqs. (20) - (22). It is important to highlight that the equations used to calculate the maximum lift and drag coefficients for the post-stall ($CL2_{max}$ and $CD2_{max}$) were empirically obtained, and are given as a function of the aspect ratio (AR) and airfoil's thickness-to-chord ratio (t/c).

$$CL2 = -0.032(\alpha - 92) - RCL2 \cdot \left(\frac{92 - \alpha}{51} \right)^{N_2}, \quad \textbf{if } ACL1 \leq \alpha \leq 92^o \tag{20}$$

$$CL2 = -0.032(\alpha - 92) - RCL2 \cdot \left(\frac{\alpha - 92}{51} \right)^{N_2}, \quad \textbf{if } \alpha \geq 92^o \tag{21}$$

where $RCL2 = 1.632 - CL1_{max}$, $N_2 = 1 + \frac{CL2_{max}}{RCL2}$, $CL2_{max} = F1 \cdot F2$, $F1 = 1.190(1 - (t/c)^2)$, and $F2 = 0.65 + 0.35 \cdot e^{-(9/AR)^{2.3}}$.

$$CD2 = CD1_{max} + (CD2_{max} - CD1_{max}) \cdot \sin\left(\frac{\alpha - ACD1}{90 - ACD1} \cdot 90 \right), \quad \textbf{if } \alpha \geq ACD1 \tag{22}$$

where $CD2_{max} = G1 \cdot G2$, $G1 = 2.27 \cdot e^{-0.65(t/c)^{0.9}}$, and $G2 = 0.52 + 0.48 \cdot e^{-(6.5/AR)^{1.1}}$.

It is important to comment that in order to accurately reproduce the tests presented by Spera (2008), the $G1$ equation underwent a small change from $G1 = \mathbf{2.3} \cdot e^{-0.65(t/c)^{0.9}}$ to $G1 = \mathbf{2.27} \cdot e^{-0.65(t/c)^{0.9}}$. A detailed discussion of such change can be found in the manual of Aerodas spreadsheet, proposed by Erturk (2018). Additional details about the Aerodas model can be obtained in Spera (2008).

3. RESULTS

The starting point for a turbine simulation is the blade geometry description, as detailed as possible. Table 3 presents the blade geometry description, in 1:25 scale of the SeaGen turbine, a 2-bladed turbine ($B = 2$) with aerodynamic profile NACA 63-618. Such information is essential for the BEM application, which will occur in QBlade software.

It is important to note that the sections whose shape was a transition between the circle and the foil (NACA 63-618) were not considered. It is necessary, because in the QBlade software each inserted section must be related to a curve of $C_D \times \alpha$ and $C_L \times \alpha$ and such curves are known only for circular sections or for known aerodynamic profile.

Table 3. Blade geometry (Rahimian *et al.*, 2018).

Section	r/R	c/R	t/c [%]	$Twist$ [^{o}]	$Shape$	r [m]	c [m]	$r - R_{rub}$ [m]
1	0.102	0.080	100	12.9	circle	0.04102	0.032	0
2	0.115	0.080	100	12.9	circle	0.046	0.032	0.00498
3	0.355	0.158	18	9.5	foil	0.142	0.0632	0.10098
4	0.385	0.153	18	8.7	foil	0.154	0.0612	0.11298
5	0.445	0.145	18	7.4	foil	0.178	0.0580	0.13698
6	0.475	0.141	18	6.9	foil	0.190	0.0564	0.14898
7	0.505	0.137	18	6.5	foil	0.202	0.0548	0.16098
8	0.565	0.128	18	5.7	foil	0.226	0.0512	0.18498
9	0.595	0.124	18	5.4	foil	0.238	0.0496	0.19698
10	0.625	0.119	18	5.1	foil	0.250	0.0476	0.20898
11	0.685	0.110	18	4.5	foil	0.274	0.0440	0.23298
12	0.715	0.106	18	4.3	foil	0.286	0.0424	0.24498
13	0.745	0.101	18	4.0	foil	0.298	0.0404	0.25698
14	0.805	0.092	18	3.6	foil	0.322	0.0368	0.28098
15	0.835	0.087	18	3.4	foil	0.334	0.0348	0.29298
16	0.895	0.078	18	2.9	foil	0.358	0.0312	0.31698
17	0.925	0.073	18	2.7	foil	0.370	0.0292	0.32898
18	0.985	0.063	18	2.2	foil	0.394	0.0252	0.35298
19	1.000	0.060	18	2.1	foil	0.400	0.0240	0.35898

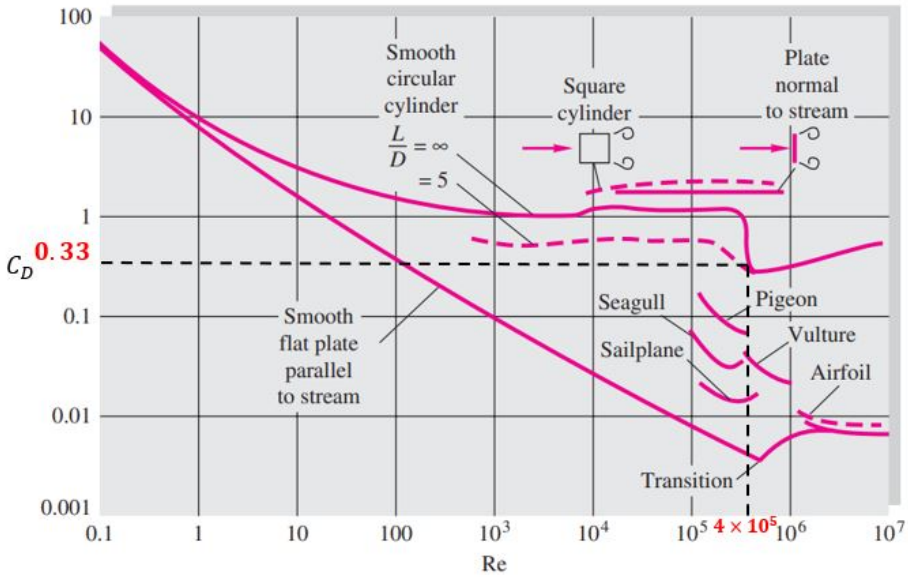

Figure 4. Procedure to obtain the C_D of circular sections.

For circular sections, $C_L = 0$ and the value of C_D is extracted from the graph of the drag coefficient as a function of the Reynolds number proposed by White (2011). The value of $C_D = 0.33$ was obtained through the intersection between the curve for smooth cylinders ($L/D = \infty$) and the Reynolds number at 70% of the blade span (s), which, according to Walker *et al.* (2014), for the present study is $Re_{c,70\%.s} = 4.0 \times 10^5$. Such procedure is presented in Fig. 4.

For the NACA 63-618 profile, it is necessary to check which of the four meshes described in Tab. 1 will be used in the simulations in the UNSCYFL3D software. Considering the Reynolds number equal to $Re_{c,70\%.s} = 4.0 \times 10^5$, meshes 1 and 3 were simulated for $\alpha = -5^o, 0^o, 5^o,\ and\ 10^o$ and meshes 2 and 4 for $\alpha = 0^o\ and\ 10^o$. Analyzing the results shown in Fig. 5, it is noted that the meshes whose spacings followed that proposed by Coder (2018), presented results closer to the reference than the mesh with $y^+ = 1$. Thus, as the results between meshes 2, 3 and 4 did not show significant differences, it was decided to apply mesh 3 in the simulation, as it is a medium mesh (less number of points than mesh 4) and has a smaller domain ($A = 20$ and $B = 25$).

The results of the steady-state simulations in UNSCYFL3D for the NACA 63-618 profile with mesh 3 and LM-SST turbulence model are presented in Fig. 6 and show a good approximation to the experimental values. The simulated

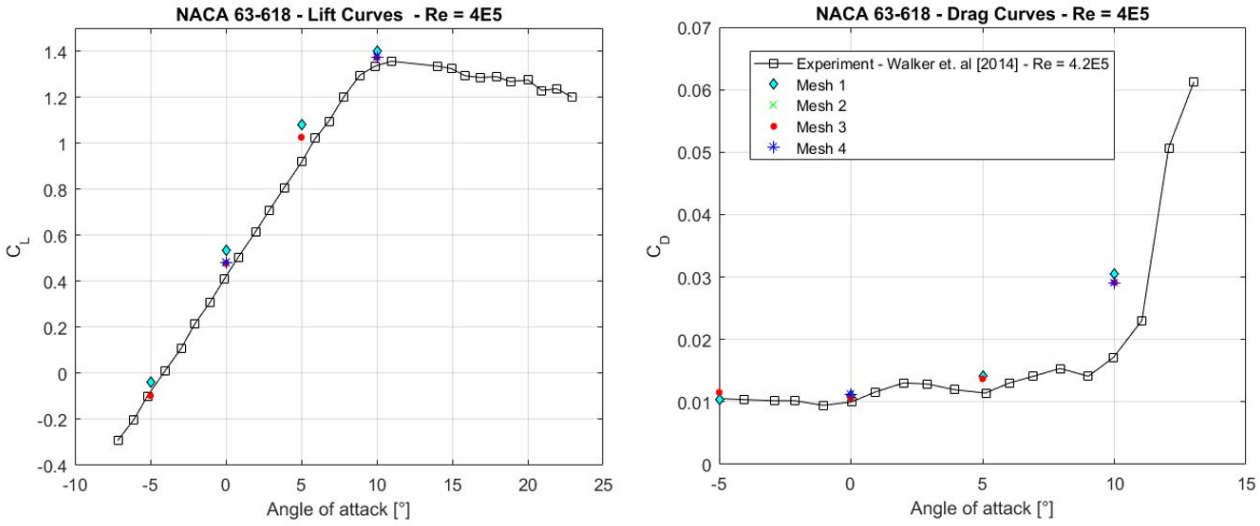

Figure 5. Mesh comparison.

angles of attack were $-5^o \leq \alpha \leq 17^o$. As the Aerodas model uses only parameters extracted from the curve of drag and lift coefficients until the stall, so the simulations could stop at $\alpha \approx 12^o$, as it was already possible to identify that $\alpha_{stall} = 10^o$. However, it was preferred to proceed as long as the results of the steady-state simulations did not present large fluctuations.

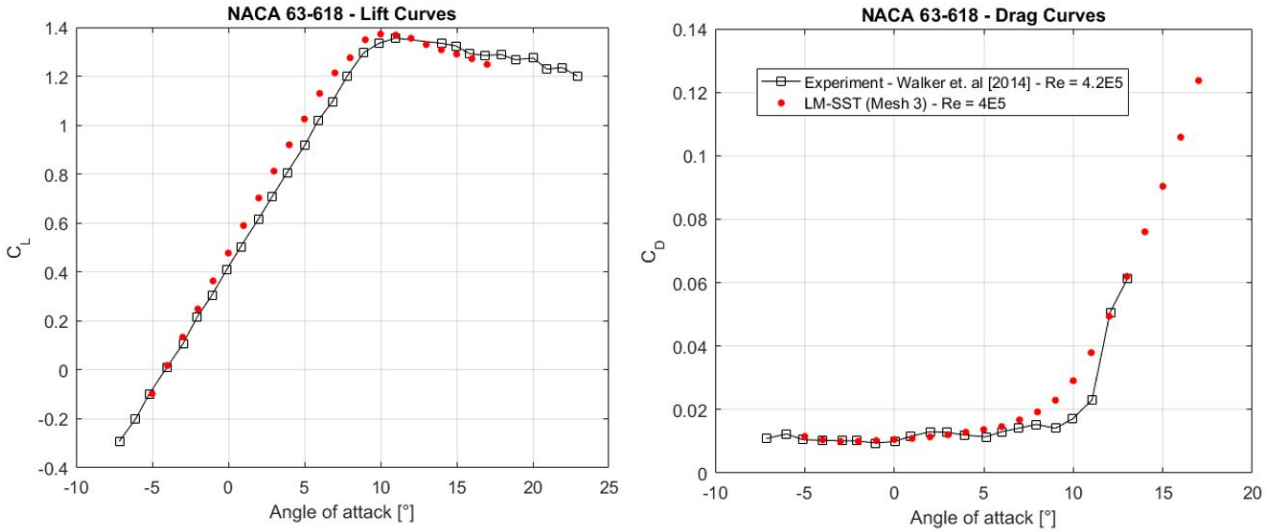

Figure 6. Lift and drag curves obtained by simulation.

Considering the simulated data for the NACA 63-618 profile until $\alpha = 10^o$, the Aerodas model was applied. The data extracted from the pre-stall curves and the curves $C_D \times \alpha$ and $C_L \times \alpha$ after treatment with the Aerodas model are shown in Tab. 4 and Fig. 7, respectively. Figure 7 also shows that the authors chose the exponent $M = 8$, based on the adjustment of Eq. (19) with graph $\frac{C_L}{C_D} \times \alpha$. This same procedure was performed for: simulated data until $\alpha = 17^o$ and experimental data until $\alpha = 10^o$ and $\alpha = 23^o$. For all calculations $AR = 12.8744$.

Estimates for the power coefficient (C_P), shown in Fig. 8, are close to the reference and prove the validity of the proposed procedure. Analyzing the results, no substantial differences were observed when using a greater amount of data, so the ideal is that the curves of drag and lift coefficients are determined until $\alpha = \alpha_{stall}$, because this requires a minimum of experimental or simulated data. Furthermore, for many airfoils only pre-stall data are available, as obtaining post-stall data can be quite complicated. It is essential to highlight that in addition to the corrections for the tip and root loss, the foil interpolation was also applied due to the long transition section between the circular and profiled sections (sections 2 and 3 - see Tab. 3), as presented in Fig. 9. When this interpolation is turned on, the data of an element used in the calculation is a linear interpolation of the bounding sections data (Marten and Wendler, 2018).

Table 4. Input parameters for Aerodas model aplication on lift and drag simulated data until $\alpha = 10^o$.

Parameter	Value
A0	-4.1547^o
$CL1_{max}{}'$	1.3720
ACL1$'$	10.0^o
CD0	0.0106
$CD1_{max}{}'$	0.0291
ACD1$'$	10.0^o
$S1'$	0.1109 [1/^{o}]

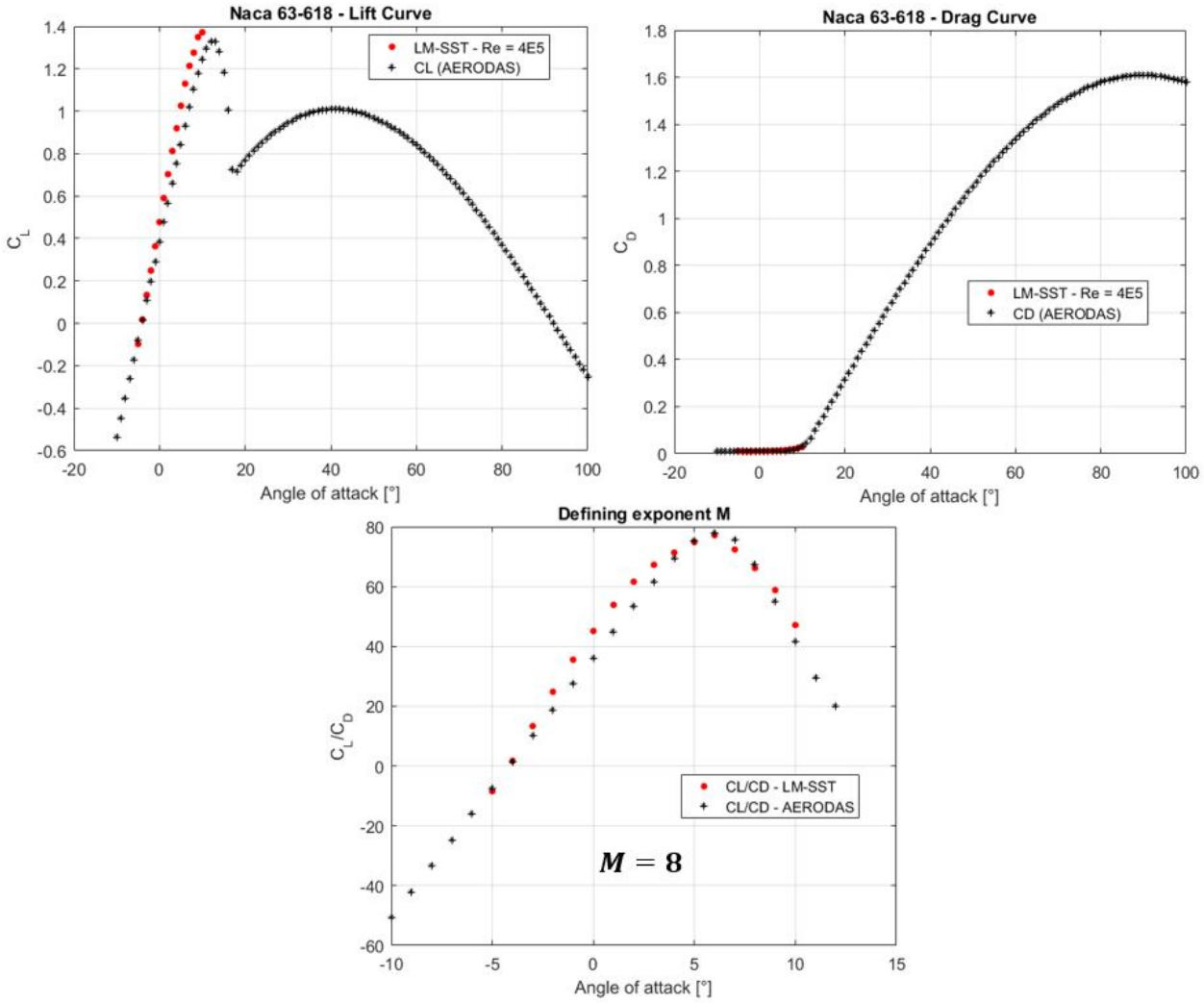

Figure 7. Treatement with Aerodas model for lift and drag simulated data until $\alpha = 10^o$.

4. CONCLUSION

All the necessary steps to carry out a relatively simple and low cost evaluation of the turbine power coefficient were detailed in the present study.

The first is to obtain the curves $C_D \times \alpha$ and $C_L \times \alpha$ for the aerodynamic profile used in the turbine, which are fundamental for the BEM application. Such curves were obtained for the NACA 63-618 profile by simulation, applying the LM-SST transitional turbulence model, as suggested by Ignacio *et al.* (2020). The mesh was built adopting the spacing proposed by Coder (2018), which are given as a function of the profile chord length (c), being that a remarkable point. Another interesting point is that for circular shape section, was considered $C_L = 0$ and C_D was obtained from the graph $C_D \times Re$ proposed by White (2011).

Posteriorly, the simulated data of C_D and C_L were treated with the Aerodas model and inserted into the QBlade

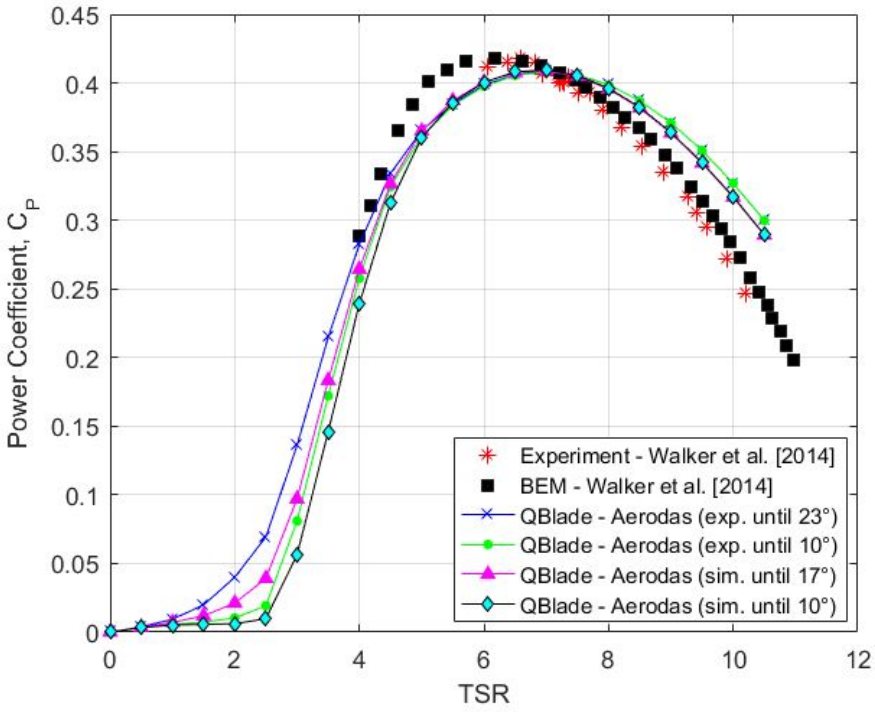

Figure 8. Power coefficient estimation.

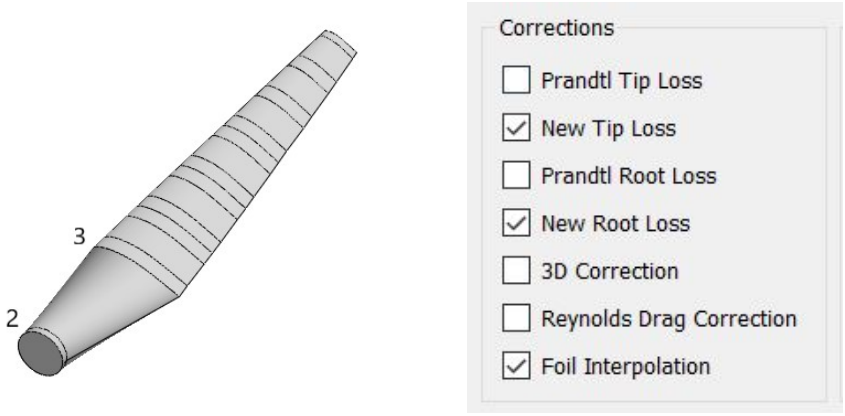

(a) Blade view on QBlade. (b) Corrections applied.

Figure 9. Corrections applied on QBlade software.

software to obtain the power coefficient as a function of the TSR. The results obtained for the C_P showed that using a larger amount of data for the application of the Aerodas model did not generate appreciable differences in the estimates. In other words, values for C_D and C_L until α_{stall} are sufficient. Such result should be underlined, as the data present in the literature are generally for $\alpha \leq \alpha_{stall}$, since performing experiments or simulations for $\alpha > \alpha_{stall}$ is usually quite complex. It is also important to highlight the need to apply the foil interpolation with tip and root loss correction, due to the long transition length from blade root to the section with airfoil shape.

5. ACKNOWLEDGEMENTS

The authors are thankful to the Coordination for the Improvement of Higher Education Personnel (CAPES), Brazilian Research Council (CNPq), Ferderal University of Uberlândia, and the Goiano Federal Institute (IF Goiano).

6. REFERENCES

AirfoilTools, 2022. “Naca 63(3)-618”. <http://airfoiltools.com/airfoil/details?airfoil=naca633618-il.
Bai, C.J. and Wang, W.C., 2016. “Review of computational and experimental approaches to analysis of aerodynamic

performance in horizontal-axis wind turbines (HAWTs)". *Renewable and Sustainable Energy Reviews*, Vol. 63, pp. 506–519.

Barnes, R., Morozov, E. and Shankar, K., 2015. "Improved methodology for design of low wind speed specific wind turbine blades". *Composite Structures*, Vol. 119, pp. 677–684.

Branlard, E., 2017. *Wind Turbine Aerodynamics and Vorticity-Based Methods*. Research Topics in Wind Energy. Springer Cham.

Cao, H., 2011. "Aerodynamics analysis of small horizontal axis wind turbine blades by using 2D and 3D CFD modelling".

Carcangiu, C.E., 2008. "CFD-RANS study of horizontal axis wind turbines".

Coder, J.G., 2018. *Standard Test Cases for CFD-Based Laminar-Transition Model Verification and Validation*.

Erturk, E., 2018. "A spreadsheet tool for the aerodas model for calculating airfoil pre-stall and post-stall lift and drag characteristics". *International Journal of Renewable Research*, Vol. 8, pp. 2180–2189.

Fingersh, L., Hand, M. and Laxson, A., 2006. "Wind turbine design cost and scaling model. national renewable energy laboratory - nrel/tp-500-40566". Technical report, National Renewable Energy Laboratory - NREL/TP-500-40566.

Ignacio, L.H.S., Duarte, C.A.R. and Souza, F.J., 2020. "Simulation of laminar-to-turbulent transitional flow over airfoils". *Proceedings of XII Spring School of Transition and Turbulence*.

Ingram, G., 2005. "Wind turbine blade analysis using the blade element momentum method." Technical report, School of Engineering - Durham University.

Lanzafame, R., Mauro, S. and Messina, M., 2013. "Wind turbine CFD modeling using a correlation-based transitional model". *Renewable Energy*, Vol. 52, pp. 31–39.

Lanzafame, R. and Messina, M., 2007. "Fluid dynamics wind turbine design: Critical analysis, optimization and application of BEM theory". *Renewable Energy*, Vol. 32, pp. 2291–2305.

Liu, X., Lu, C., Liang, S., Godbole, A. and Chen, Y., 2017. "Vibration-induced aerodynamic loads on large horizontal axis wind turbine blades". *Applied Energy*, Vol. 185, pp. 1109–1119.

Manwell, J.F., McGowan, J.G. and Rogers, A.L., 2002. *Wind Energy Explained: Theory, Design and Application*. John Wiley & Sons Inc., 2nd edition.

Marten, D. and Wendler, J., 2018. "Qblade guidelines - v0.6". Technical report, Technische Universität Berlin.

Marten, D., Wendler, J., Pechlivanoglou, G., Nayeri, C. and Paschereit, C., 2013. "Qblade: An open source tool for design and simulation of horizontal and vertical axis wind turbines". *International Journal of Emerging Technology and Advanced Engineering*, Vol. 3, pp. 264–269.

Montgomerie, B., 2004. "Methods for root effects, tip effects and extending the angle of attack to $\pm 180^o$ with application to aerodynamics for blades on wind turbines and propellers". Technical report, Swedish Defence Research Agency, FOI-R–1305—SE.

Pratumnopharat, P. and Leung, P.S., 2011. "Validation of various windmill brake state models used by blade element momentum calculation". *Renewable Energy*, Vol. 36, pp. 3222–3227.

Puraca, R.C., 2019. *Análise de estratégias de controle e otimização de turbinas eólicas considerando degradação da superfície das pás*. Master's thesis, Universidade de São Paulo, São Paulo.

Rahimian, M., Walker, J. and Penesis, I., 2018. "Performance of a horizontal axis marine current turbine– a comprehensive evaluation using experimental, numerical, and theoretical approaches". *Energy*, Vol. 148, pp. 965–976.

Sezer-Uzol, N. and Long, L.N., 2006. "3-D time-accurate CFD simulations of wind turbine rotor flow fields". *44th AIAA Aerospace Sciences Meeting and Exhibit*.

Song, Q. and Lubitz, W.D., 2013. "BEM simulation and performance analysis of a small wind turbine rotor". *Wind Engineering*, Vol. 37, pp. 381–399.

Spera, D.A., 2008. "Models of lift and drag coefficients of stalled and unstalled airfoils in wind turbines and wind tunnels". Technical report, National Aeronautics and Space Administration - NASA/CR—2008-215434.

Viterna, L.A. and Janetzke, D.C., 1982. "Theoretical and experimental power from large horizontal-axis wind turbines". Technical report, National Aeronautics and Space Administration - NASA TM-82944.

Walker, J.M., Flack, K.A., Lust, E.E., Schultz, M.P. and Luznik, L., 2014. "Experimental and numerical studies of blade roughness and fouling on marine current turbine performance". *Renewable Energy*, Vol. 66, p. 257–267.

White, F.M., 2011. *Fluid Mechanics*. McGraw-Hill, 6th edition.

7. RESPONSIBILITY NOTICE

The authors are the only responsible for the printed material included in this paper.